Chemically Stable Polyarylether-Based Metallophthalocyanine Frameworks with High Carrier Mobilities for Capacitive Energy Storage

Chongqing Yang,[1#] Kaiyue Jiang,[2#] Qi Zheng,[3] Xinle Li,[1,4] Haiyan Mao,[5] Wenkai Zhong,[1,2] Cheng Chen,[2] Bing Sun,[1,6] Haimei Zheng,[3] Xiaodong Zhuang,[2] Jeffery A. Reimer,[3,5] Yi Liu,[1] and Jian Zhang[1*]

1. The Molecular Foundry, Lawrence Berkeley National Laboratory, Berkeley, California 94720, United States

2. School of Chemistry and Chemical Engineering, Shanghai Jiao Tong University, Shanghai 200240, P.R. China

3. Materials Sciences Division, Lawrence Berkeley National Laboratory, Berkeley, California 94720, United States

4. Department of Chemistry, Clark Atlanta University, Atlanta, Georgia 30314, United States

5. Department of Chemical and Biomolecular Engineering, University of California, Berkeley, California 94720, United States

6. School of Science, China University of Geosciences (Beijing), Beijing 100083, P.R. China

ABSTRACT: Covalent organic frameworks (COFs) with efficient charge transport and exceptional chemical stability are emerging as an importance class of semiconducting materials for opto-/electronic devices and energy related applications. However, the limited synthetic chemistry to access such materials and the lack of mechanistic understanding of carrier mobility greatly hinder their practical applications. Herein, we report the synthesis of three chemically stable polyarylether-based metallophthalocyanine (PAE-PcM, M = Cu, Ni, and Co) COFs and facile *in-situ* growth of their thin films on various substrates (e.g., SiO_2/Si, ITO, quartz) under solvothermal conditions. We show that PAE-PcM COFs thin films with van der Waals layered structures exhibit *p*-type semiconducting properties with the intrinsic mobility up to ~19.4 $cm^2 V^{-1} s^{-1}$ and four orders of magnitude of increase in conductivity (0.2 S m^{-1}) after iodine doping. Density functional theory (DFT) calculations reveal that the carrier transporting in the framework is anisotropic, with the out-of-plane hole transporting along columnar stacked phthalocyanine more favorable. Furthermore, PAE-PcCo shows the redox behavior maximumly contributes ~88.5% of its capacitance performance, yielding a high surface area normalized capacitance of ~19 μF cm^{-2}. Overall, this work not only deepens the understanding of electronic properties of polyarylether-based 2D COFs and but also opens new opportunities for their integration into various microdevices for energy storage applications.

INTRODUCTION

Covalent organic frameworks (COFs) with inherent chemical tunability, ordered supramolecular lattices, and tailorable nano-porosity[1-3] have emerged as a unique class of functional crystalline materials, finding applications in gas/chemical storage and separation,[4-6] drug delivery,[7] chemo-sensing,[8-9] catalysis,[10] etc. In recent years, high charge carrier mobility has also been successfully realized in a number of two-dimensional (2D) COFs which exhibit outstanding (opto)electronic properties.[11-14] In order to broaden their real applications in memory devices,[15-17] photo-/electrocatalyses,[18-21] chemiresistors,[22-23] energy storage,[24-25] among others, imparting chemical robustness in these 2D COFs is of imperative importance. Synthetic chemistry to construct robust 2D COFs with high charge carrier mobility is limited, with only a few reported examples using pyrazine[22, 26-27] or olefin[28] as the linkages. Recently, a new class of chemically stable 2D COFs based on the polyarylether (or dioxin) linkage was reported.[29-32] The fully planar polyarylether linkage is able to facilitate the AA-orientated stacking of planar building blocks such as triphenylene[29-30] and phthalocyanine.[31-32] It is expected that the π-stacking in these robust frameworks would facilitate numerous low-barrier carrier pathways; however, the impact of the

weakened in-plane conjugation at the polyarylether linkage on the overall carrier transporting performance is unknown. Thus, a thorough understanding of intrinsic carrier transporting behavior in these polyarylether-linked COFs is warranted.

One the other hand, besides chemical structure, the physical form of 2D COFs also plays an important role in evaluating their carrier mobilities.[33-37] Compared with bulk powders, continuous, oriented COF thin films could potentially reduce the interference of grain boundary resistance on their intrinsic (opto)electronic properties.[12] In the past few years, preparation of free-standing and polycrystalline COF thin films has been made possible via air-liquid[38] and liquid-liquid[39-40] interfacial synthesis. However, most mobility-evaluating device fabrications based on these films require harsh processing procedures, such as metal electrode deposition at high vacuum/temperature and wet-chemistry mask etching.[15] These complicated operations can lead to cracking or even exfoliation of the crystalline thin films from substrates.[41-42] Therefore, improving the compatibility of COF thin films with applied substrates while retaining their crystallinity remains a crucial task.

Herein, we report the synthesis of three chemically stable polyarylether-based metallophthalocyanine (PAE-PcM) COFs and the facile *in-situ* growth of their thin films on various substrates (e.g., SiO_2/Si, ITO, quartz) under solvothermal conditions. Despite the weakened in-plane π-conjugation, the PAE-PcM COFs thin films with van der Waals layered structures exhibit *p*-type semiconducting properties with high mobilities up to 19.4 $cm^2 V^{-1} s^{-1}$. The intrinsic conductivity of 3.8×10^{-5} S m^{-1} for PAE-PcCu film can increase by four orders of magnitude to 0.2 S m^{-1} after iodine doping. DFT calculations reveal that the columnar stacking of phthalocyanine macrocycles mostly contribute to the overall carrier transporting properties and consequently the exceedingly small bandgaps. Furthermore, PAE-PcCo exhibits a high surface area normalized capacitance of ~19 μF cm^{-2} and a good long-term durability. Overall, this work not only deepens the understanding of electronic properties of polyarylether-based 2D COFs but also opens new opportunities for their integration into various microdevices for energy storage applications.

RESULTS AND DISCUSSION

The three PAE-PcM COFs (M = Cu, Ni, and Co) were constructed through the condensation reaction of (2,3,9,10,16,17,23,24-octahydroxylphthalocyaninato)metal(II) ($PcMOH_8$) and tetrafluoroterephthalonitrile (TFPN) (Figure 1a and Supporting Information). Their crystal structure was firstly characterized by the wide-angle X-ray scattering (WAXS) in combination with density functional theory (DFT) calculations. As shown in Figure 1b, the strong distinct diffraction peaks at 4.57°, 9.39°, and 27.15° for PAE-PcCu can be assigned to the (100), (200), and (001) facets, respectively (Figure 1b), indicating a lamella tetragonal framework. Simulated diffraction peaks of the serrated AA stacked structure ($a = b$ = 20.19 Å, c = 3.59 Å, $\alpha = \beta = \gamma$ = 90°) are in good agreement with experimental diffraction peaks (Figure 1b and S1-3). In addition, the broad peak at 27.15° corresponds to the (001) facet with interlayer distance of ~3.3 Å. PAE-PcNi and PAE-PcCo also exhibit a similar tetragonal layered structure in the serrated AA stacking mode (Figure S3-4). High resolution transmission electron microscopy (HRTEM) of PAE-PcCu and its corresponding fast Fourier transform (FFT) analysis further evidence the square lattices with $a = b$ = ~2 nm, which are in well consistence with the WAXS analysis (Figure 1c). The corresponding elemental mappings demonstrate the aggregated particles in as-made powders and the homogeneous distribution of carbon, nitrogen, oxygen, and metal elements throughout the frameworks (Figures S6-8).

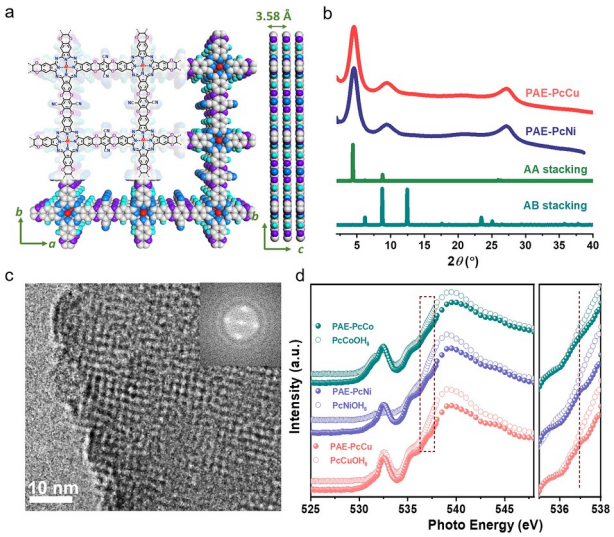

Figure 1. (a) Top (*ab* plane) and side (*bc* plane) view of the simulated crystal structure of PAE-PcCu with serrated AA stacking. (b) Experimental WAXS pattern for PAE-PcCu (red), PAE-PcNi (purple) and simulations based on serrated AA (green) and AB (dark cyan) stacking (λ = 1.54 Å). (c) High resolution TEM images of PAE-PcCu. Inset: corresponding fast Fourier transform (FFT) result. (d) Oxygen K-edge XANES spectra for PAE-PcM and PcMOH8.

The successful formation of ether bond was confirmed by the new peaks centered at ~1260 and ~1040 cm^{-1} for PAE-PcM COFs in the Fourier-transform infrared (FTIR) spectra (Figure S9).[30] To further probe the chemical environment of oxygen, *K*-edge X-ray absorption near edge spectroscopy (XANES) was employed, and a new feature around 536.7 eV can be assigned to the transitions from the *1s* electron of the central

oxygen to the *2pπ** (O *1s*-*πp**; C-O-C).[43-44] In addition, the broad peak centered at 544 eV corresponds with the O *1s*-*σs** (C-O) excitation.[45] X-ray photoelectron spectroscopy (XPS) also revealed the presence of C, N, O, metal atoms as well as a trace amount of F (Figures S10-12). From the content of residue F, the conversions of the polycondensation reaction were calculated as 75.6%, 84.5%, and 74.8% for PAE-PcCu, -PcNi, and -PcCo, respectively.[30] Deconvolution of the O(*1s*) signal for PAE-PcCu generates two peaks centered at 532.7 and 533.8 eV, which can be attributed to the aromatic C-O-C bond and adsorbed H_2O/CO_2 from atmosphere (Figures S13).[46] The core level spectrum of Cu(*2p*) resembled that of $PcCuOH_8$ with two dominant peaks at 940.0 eV (Cu $2p_{3/2}$) and 954.9 eV (Cu $2p_{1/2}$), which indicates the presence of Cu(II) in the tetragonal framework (Figure S14). Analogous results from deconvolution of O(*1s*) and transition metal atoms (*2p*) were obtained for PAE-PcNi and PAE-PcCo (Figures S15-16), respectively.

The porosity of PAE-PcM was further measured by nitrogen sorption at 77 K, and all isotherms show sharp uptakes at low pressure range (P/P_0 < 0.05), indicating the microporous nature for the frameworks (Figure S17). The Brunauer-Emmett-Teller surface areas (SA_{BET}) were calculated to be 321, 398 and 367 $m^2 \cdot g^{-1}$ for PAE-PcCu, -PcNi, and -PcCo, respectively. The related pore size distribution demonstrates an average pore size of ~1.4 nm (Figure S18 and Table S1). Due to the ultra-stable polyarylether linkages, the obtained COFs showed great robustness with no apparent loss of crystallinity was observed after the treatment under harsh conditions such as polar solvent in NMP (*N*-methyl-2-pyrrolidone), boiling water, concentrated HCl (12 M) and KOH (7 M and 14 M) solutions (Figures S19-20).

Owing to the small distance (~3.3 Å) between the close-packed phthalocyanine rings, it is believed that considerable carrier transport could occur in PAE-PcM COFs. DFT calculation was first employed to study the intrinsic electronic band structures of PAE-PcM COFs. The electronic band structure and the projected density of states (PDOS) for monolayer and bulk models of PAE-PcCu were first calculated (Figure 2a-c), and the band structure of the monolayer shows the typical semiconducting feature with a direct bandgap of ~1.33 eV. The relative flat conduction band (CB) and valence band (VB) indicate that the charge transport along the 2D plane is relatively null due to the localized electron density trapped within the phthalocyanine moiety. Notably, the stacked multi-layer structure (along Γ-X, M-Γ, Figure 2b and 2d) showed slight improved band dispersion with a moderate bandgap of ~ 0.94 eV. In contrast, the band structures of bulk PAE-PcCu (along Z-A, M-Γ, Z-R, X-Γ; Figure 2c and 2d) demonstrated a distinct reduced bandgap of 0.46 eV with appreciable band dispersion. These results indicate that the charge transport in bulk PAE-PcCu is anisotropic and the pathways from interlayer *π*-*π* interactions are much more favorable to the carrier mobility due to the formation of periodic *π*-columns.[22, 47] The average carrier effective mass along the out-of-plane direction were calculated to be m_h = 1.2 m_0^* and m_e = 1.5 m_0^* for holes and electrons, respectively, further suggests the conductivity in the out-of-plane direction is more favorable. Bulk PAE-PcNi and PAE-PcCo also demonstrate similar indirect bandgaps of 0.52 eV and 0.51 eV, respectively (Figure S21-22). Taking together, the DFT calculation reveals that the metal center has a neglectable effect on the electronic band-structures on PAE-PcM COFs.[26]

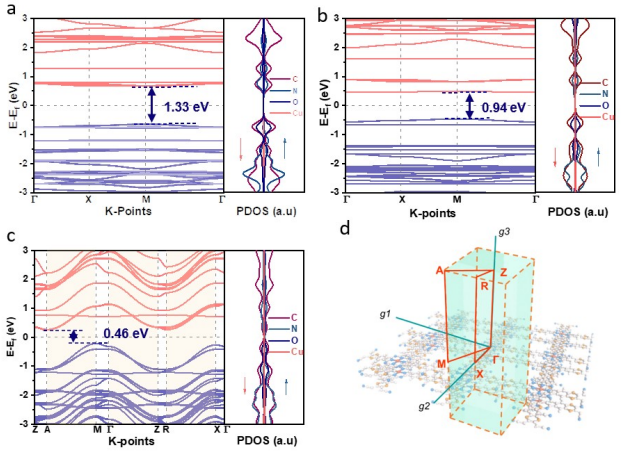

Figure 2. (a) Calculated band structure of a monolayer PAE-PcCu with GGA+U correction and the corresponding projected density of states (PDOS) for C (p), N(p), O(p) and Cu(d) states (red arrow: spin-down; blue arrow: spin-up). (b) Electronic band structure of serrated AA stacked PAE-PcCu layers along the in-plane high symmetry K-points. (c) Calculated band structure of bulk PAE-PcCu along in-plane and out-of-plane high symmetry K-points. The light-yellow regions are pathways along the out-of-plane directions. (d) Corresponding first Brillouin zone and high symmetry K-points.

Next, the charge mobility behavior of PAE-PcM frameworks was analyzed experimentally. In consideration of the challenges posed by the numerous grain boundaries of bulk COF powders, the direct growth of oriented thin films of PAE-PcM on confined interfaces was explored to reveal their intrinsic electronic properties. The PAE-PcM films were prepared on ITO, quartz, and Si/SiO_2 substrates via solvothermal reactions (Figure 3a and Figure S23, see Supporting Information for detailed synthesis procedure). Their morphologies were characterized by the optical microscopy (OM), scanning electron microscopy (SEM), and atomic force microscopy (AFM). The OM and SEM images demonstrated that all films are continuous with microscopic lateral size of several millimeters (Figure 3b and S24). Tapping mode AFM was then used to characterize the obtained thin films, and based on the cross-sectional analysis, and the average thicknesses of PAE-

PcCu, PcNi, and PcCo are 46, 86, and 78 nm, respectively (Figure S25). The grazing-incidence wide-angle X-ray scattering (GIWAXS) studies further confirmed the formation of crystalline COF thin films. As shown in Figure 2c-d, the corresponding GIWAXS patterns for PAE-PcCu thin film showed strong reflections at ~ 0.42, 0.75, and 1.60 $Å^{-1}$ with the corresponding *d*-spacings of 18.4, 9.0, and 3.5 Å, respectively, indicating the successful formation of layered tetragonal lattices of PAE-PcCu with an interlayer *d*-spacing of 3.5 Å on confined interfaces, consistent with the PXRD result of the bulk powder sample. Similar results were obtained for PAE-PcNi and PAE-PcCo with slightly reduced crystallinity (Figure S26-27).

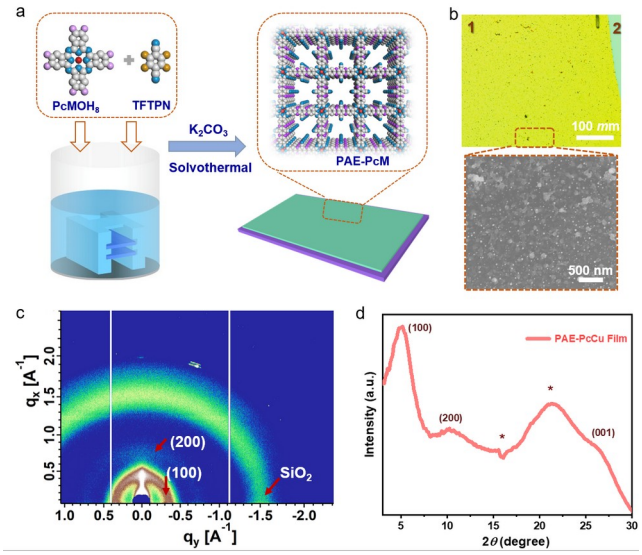

Figure 3. (a) Schematic illustration of in-situ growth of PAE-PcM films on different substrates via solvothermal reactions. (b) Optical microscope image of PAE-PcCu and the corresponding SEM image, indicating the homogeneous and continuous film. (c) The GIWAXS pattern of PAE-PcCu thin films grown on SiO_2/Si. (d) Corresponding 1D XRD curve converting from the GIWAXS result (λ = 1.54 Å). Asterisks indicate the SiO_2 signals.

The optoelectronic properties of the PAE-PcM films were then evaluated by the UV/vis spectroscopy and cyclic voltammetry (CV). As shown in Figure S28, typical Q band (~700 nm) and B band (~416 nm) were observed for all three films (on quartz). The corresponding indirect optical bandgaps were calculated to be 1.27, 1.42, and 1.50 eV for PAE-PcCo, -PcNi, and -PcCu, respectively (Figure 4a). Electrochemical bandgaps from CV measurements show similar values for PAE-PcCo (1.29 eV), PAE-PcNi (1.40 eV) and PAE-PcCu (1.22 eV), as shown in Figure 4b and S29. To evaluate their carrier mobility, Hall effect measurements were conducted at room temperature after depositing four gold electrodes on the top of the COF films on Si/SiO_2 (Figure S30). The results reveal that all PAE-PcM COFs are *p*-type semiconductors with inferred average charge carrier densities of $7.2(\pm1.8)\times10^{12}$, $2.4(\pm1.5)\times10^{12}$, and $0.7(\pm0.4)\times10^{12}$ cm^{-3} for PAE-PcCu, -PcNi and -PcCo, respectively. The corresponding Hall mobility in the *dc* limit shows that PAE-PcCo has the highest carrier mobility of ~19.4 (±5.1) $cm^2\ V^{-1}\ s^{-1}$, while the carrier mobility of PAE-PcNi and PAE-PcCu are 3.2(±1.9) and $3.2(\pm0.2)\times10^{-1}$ $cm^2\ V^{-1}\ s^{-1}$, respectively (Figure S31). These results show that the tetragonal framework with the cobalt center exhibits the best transporting performance that ranks among state-of-art COF semiconductors (Table S2). Notably, the difference in mobility among the three PAE-PcM COFs could be attributed to the intrinsic difference of the metal centers and some extrinsic factors such as grain boundary diffraction, crystalline domain orientation, etc.. We also measured the electrical dc conductivity of the as-made PAE-PcCu film via a two-probe method and observed a linear current−voltage (*I*−*V*) relationship, and a conductivity of $\sim3.8\times10^{-5}$ S m^{-1} with nearly ohmic behavior at room temperature was obtained (Figures 3d and S32-33). This value is comparable with previous reported phthalocyanine-based COFs such as CuPc-pz[26] (3.3×10^{-5} S m^{-1}) and NiPc-CoTAA[23] (8.2×10^{-3} S m^{-1}). Notably, after iodine doping, a significant increase of four orders of magnitude with the conductivity reaching 0.2 S m^{-1}could be observed.

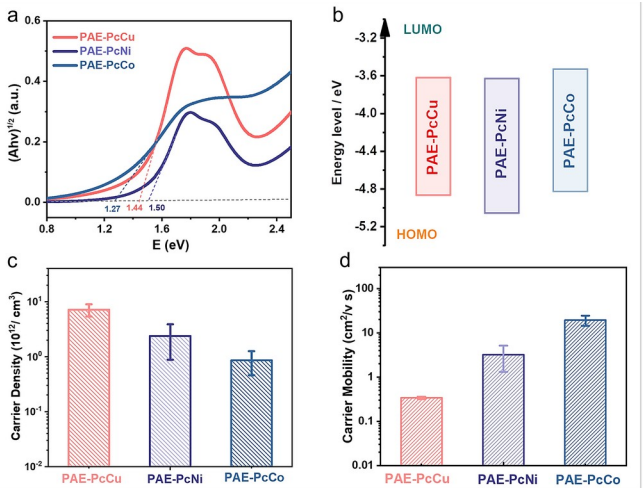

Figure 4. (a) Tauc plots of PAE-PcM thin films. (b) Experimental HOMO and LUMO energy levels of PAE-PcM calculated from CV. (c) Average carrier density and (d) carrier mobility of PAE-PcM thin films obtained from Hall measurements.

Considering its good porosity, carrier transport property, and high chemical stability, the capacitance behavior of PAE-PcCo was further explored. Owing to its large open channels of ~1.4 nm, PAE-PcCo could accommodate large electrolyte ions, e.g., 1-ethyl-3-methyl-imidazolium ($EMIm^+$; size 0.8 nm[48]). A 3-electrode system in 0.5 M [EMIm]Cl electrolyte was used to first study the electrochemical performance. As shown in Figure S34, CV curves of PAE-PcCo showed stable potential windows both cycled

catholically (–0.6 – 0.0 V) and anodically (0.0 – 0.8 V) with three pairs of broad redox peaks at –0.2 V, 0.2 V and 0.4 V , suggesting the capacitance characteristics of PAE-PcCo in a wide potential window range of –0.6 – 0.8 V, with charge storage contribution from both electrical double layer capacitance (diffusion-controlled, C_{dl}) and pseudo-capacitance (redox process, C_p). The detailed capacitance contribution of C_{dl} and C_p were then subsequentially studied via the Dunn method[49] using a quasi-solid-state symmetric supercapacitor with [EMImCl]/acetonitrile (0.5 M) as the electrolyte. In the working window of 0–1.4 V, the CV curves at different scan rates showed similar rectangular shapes with quite broad redox peaks (Figure S35). The relationship between the current and scan rate were firstly studied at low scan rates, the corresponding b-value at different potentials were calculated to be 0.64, 0.61, 0.61, 0.65, 0.69, 0.75, and 0.85 at 0.4, 0.6, 0.8, 1.0, 1.1, 1.2, and 1.3 V, respectively. Since a *b*-value of 1.0 represents an ideal pseudocapacitive process from redox reactions, while a *b*-value of 0.5 means a diffusion-controlled process,[50] our results strongly indicate that the charge storage behavior of PAE-PcCo is contributed both from diffusion-controlled (C_{dl}) and capacitive redox process (C_p). As shown in Figure 5a, the C_p contributes a smaller fraction (~33.3%) of total capacitance behavior at 2 mV s^{-1}. As scan rate increases, the contribution of C_p increases up to 88.7% at the scan rate of 80 mV s^{-1}. Moreover, the capacitive differentiation from Trasatti analysis[51] also indicates that the maximum redox contribution is ~88.5%, which is in excellent agreement with that from Dunn analysis (Figure S36). All these results confirmed that the Faradic reactions of redox active sites in PAE-PcCo showed a dominate contribution to the total capacitive behavior.

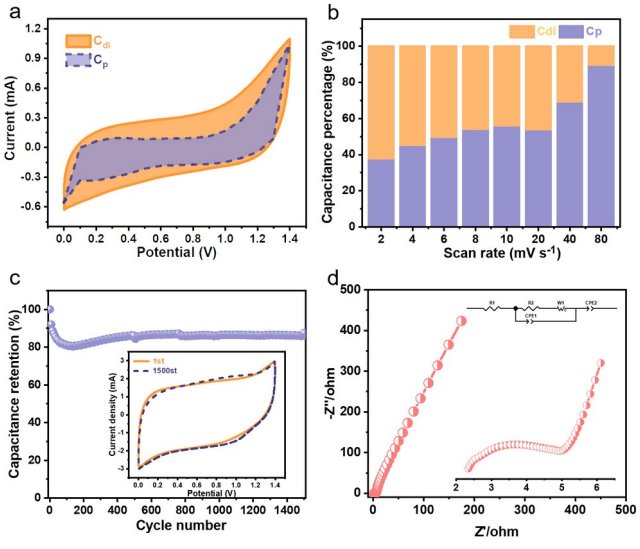

Figure 5. (a) Respective capacitance contribution of PAE-PcCo at scan rate of 2 mV s^{-1}. b) Percentage of capacitance contribution at different scan rates. c) Cycling stability test at 80 mV s^{-1}. Inset: comparison of initial and 1500th CV curve. (d) Nyquist plot. Inset: equivalent circuit of PAE-PcCo electrode (R1: solution resistance; R2: charge transfer resistance; W: Warburg impedance).

According to the CV curves, the specific capacitance was calculated to be 100 μF cm^{-2} at 2 mV s^{-1} (Figure S38). Notably, the corresponding normalized capacitance to specific surface area of PAE-PcCo is 19 μF cm^{-2}(Figure S39), apparently higher than several other pure electric double-layer capacitor materials such as active graphene (5 μF cm^{-2}; SA_{BET} = 3523 cm^2 g^{-1}),[52] single-walled CNTs (12 μF cm^{-2}; SA_{BET} = 1300 cm^2 g^{-1}),[53] and chemically reduced graphene (7 μF cm^{-2}; SA_{BET} = 2400 cm^2 g^{-1}).[54] This result further confirmed that the capacitance of PAE-PcCo are contributed mostly from the redox behavior during the energy storage process. Owing to the robust chemical stability of PAE-PcCo, the device also showed good stability, with 86% maintenance after 1500 cycles at 80 mV s^{-1} (Figure 5c). EIS profile for the solid-state supercapacitor cell exhibits an almost vertical low-frequency region in the Nyquist plot with a low equivalent Ohmic resistance of 2.2 Ω (Figure 5d and S39), which verifies a superior accessibility of ions to active sites. Thanks to the low internal resistance, intrinsic porosity, and rich redox behavior of electrode materials, the PAE-PcCo based device delivered high capacitance.

CONCLUSION

In summary, we have synthesized a series of layered polyarylether-based metallophthalocyanine frameworks. These PAE-PcM COFs demonstrate robust chemical stability and intrinsic *p*-type semiconducting behavior with high carrier mobility up to ~19.4 cm^2 V^{-1} s^{-1} and the intrinsic conductivity of PAE-PcCu film can increase by four orders of magnitude to 0.2 S m^{-1} after iodine doping. As a proof-of-concept application, PAE-PcCo COF with good carrier mobility was used as electrode for all-solid-state supercapacitors, and its capacitance behavior is mostly attributed to the redox process during charge-discharge process with a maximum contribution of 88.5%. It exhibits a high surface area normalized capacitance of ~19 μF cm^{-2} and a good long-term capacitance retention of 86% after 1500 cycles. This work deepens the understanding of electronic properties of polyarylether-based 2D COFs and opens new opportunities for their potential energy related applications.

ASSOCIATED CONTENT

Supporting Information

The Supporting Information is available free of charge on the ACS Publications website. Synthesis and characterization of PAE-PcM; DFT calculations; electrochemical performance (PDF)

AUTHOR INFORMATION

Corresponding Author

*Email: jianzhang@lbl.gov

Author Contributions

#C.Y. and K.J. contributed equally. The manuscript was written through contributions of all authors. All authors have given approval to the final version of the manuscript. C.Y. and J.Z. conceived and designed this project. C.Y. synthesized the monomers and COFs and performed the structural and morphology measurements. C.Y., X.L., Y.L. and J.Z. contributed to the discussions of the synthesis and characterization. K.J., C.Y., and X.Z. performed the DFT calculations and analysis. Q.Z. and H.Z. contributed to the TEM measurements and analysis. H.M. and J.R. contributed to the solid-state NMR characterization and analysis. W.Z. contributed to the XANES measurement. B.S. contributed to the conductivity measurements. C.C and C.Y contributed to the supercapacitor analysis. All authors discussed and revised this manuscript.

Notes

The authors declare no competing financial interest.

ACKNOWLEDGMENT

Work at the Molecular Foundry was supported by the Office of Science, Office of Basic Energy Sciences, of the U.S. Department of Energy, and by the Laboratory Directed Research and Development Program of Lawrence Berkeley National Laboratory under U.S. Department of Energy contract no. DE-AC02-05CH11231. K.J., C.C. and X.Z acknowledge the financial support from NSFC (51973114, 21720102002). This research used resources of the Advanced Light Source, a U.S. DOE Office of Science User Facility under contract no. DE-AC02-05CH11231.

REFERENCES

1. Jiang, J.; Zhao, Y.; Yaghi, O. M., Covalent Chemistry beyond Molecules. *J. Am. Chem. Soc.* **2016,** *138* (10), 3255-3265.
2. Diercks, C. S.; Yaghi, O. M., The atom, the molecule, and the covalent organic framework. *Science* **2017,** *355* (6328), eaal1585.
3. Geng, K.; He, T.; Liu, R.; Dalapati, S.; Tan, K. T.; Li, Z.; Tao, S.; Gong, Y.; Jiang, Q.; Jiang, D., Covalent Organic Frameworks: Design, Synthesis, and Functions. *Chem. Rev.* **2020,** *120* (16), 8814-8933.
4. Furukawa, H.; Yaghi, O. M., Storage of hydrogen, methane, and carbon dioxide in highly porous covalent organic frameworks for clean energy applications. *J. Am. Chem. Soc.* **2009,** *131* (25), 8875-8883.
5. Huang, N.; Chen, X.; Krishna, R.; Jiang, D., Two-dimensional covalent organic frameworks for carbon dioxide capture through channel-wall functionalization. *Angew. Chem., Int. Ed.* **2015,** *54* (10), 2986-2990.
6. Ma, Y. X.; Li, Z. J.; Wei, L.; Ding, S. Y.; Zhang, Y. B.; Wang, W., A Dynamic Three-Dimensional Covalent Organic Framework. *J. Am. Chem. Soc.* **2017**, 4995-4998.
7. Fang, Q.; Wang, J.; Gu, S.; Kaspar, R. B.; Zhuang, Z.; Zheng, J.; Guo, H.; Qiu, S.; Yan, Y., 3D Porous Crystalline Polyimide Covalent Organic Frameworks for Drug Delivery. *J. Am. Chem. Soc.* **2015,** *137* (26), 8352-8355.
8. Dalapati, S.; Jin, S.; Gao, J.; Xu, Y.; Nagai, A.; Jiang, D., An azine-linked covalent organic framework. *J. Am. Chem. Soc.* **2013,** *135* (46), 17310-17313.
9. Wu, X.; Han, X.; Xu, Q.; Liu, Y.; Yuan, C.; Yang, S.; Liu, Y.; Jiang, J.; Cui, Y., Chiral BINOL-Based Covalent Organic Frameworks for Enantioselective Sensing. *J. Am. Chem. Soc.* **2019,** *141* (17), 7081-7089.
10. Lu, S.; Hu, Y.; Wan, S.; McCaffrey, R.; Jin, Y.; Gu, H.; Zhang, W., Synthesis of Ultrafine and Highly Dispersed Metal Nanoparticles Confined in a Thioether-Containing Covalent Organic Framework and Their Catalytic Applications. *J. Am. Chem. Soc.* **2017,** *139* (47), 17082-17088.
11. Allendorf, M. D.; Dong, R.; Feng, X.; Kaskel, S.; Matoga, D.; Stavila, V., Electronic Devices Using Open Framework Materials. *Chem. Rev.* **2020,** *120* (16), 8581-8640.
12. Keller, N.; Bein, T., Optoelectronic processes in covalent organic frameworks. *Chem. Soc. Rev.* **2021,** *50* (3), 1813-1845.
13. Cai, S.-L.; Zhang, Y.-B.; Pun, A. B.; He, B.; Yang, J.; Toma, F. M.; Sharp, I. D.; Yaghi, O. M.; Fan, J.; Zheng, S.-R.; Zhang, W.-G.; Liu, Y., Tunable electrical conductivity in oriented thin films of tetrathiafulvalene-based covalent organic framework. *Chem. Sci.* **2014,** *5* (12), 4693-4700.
14. Cai, S.; Sun, B.; Li, X.; Yan, Y.; Navarro, A.; Garzón-Ruiz, A.; Mao, H.; Chatterjee, R.; Yano, J.; Zhu, C.; Reimer, J. A.; Zheng, S.; Fan, J.; Zhang, W.; Liu, Y., Reversible Interlayer Sliding and Conductivity Changes in Adaptive Tetrathiafulvalene-Based Covalent Organic Frameworks. *ACS Appl. Mater. Interfaces* **2020,** *12* (16), 19054-19061.
15. Sun, B.; Zhu, C.-H.; Liu, Y.; Wang, C.; Wan, L.-J.; Wang, D., Oriented Covalent Organic Framework Film on Graphene for Robust Ambipolar Vertical Organic Field-Effect Transistor. *Chem. Mater.* **2017,** *29* (10), 4367-4374.
16. Park, S.; Liao, Z.; Ibarlucea, B.; Qi, H.; Lin, H. H.; Becker, D.; Melidonie, J.; Zhang, T.; Sahabudeen, H.; Baraban, L.; Baek, C. K.; Zheng, Z.; Zschech, E.; Fery, A.; Heine, T.; Kaiser, U.; Cuniberti, G.; Dong, R.; Feng, X., Two-Dimensional Boronate Ester Covalent Organic Framework Thin Films with Large Single Crystalline Domains for a Neuromorphic Memory Device. *Angew. Chem., Int. Ed.* **2020,** *59* (21), 8218-8224.
17. Sun, B.; Li, X.; Feng, T.; Cai, S.; Chen, T.; Zhu, C.; Zhang, J.; Wang, D.; Liu, Y., Resistive Switching Memory Performance of Two-Dimensional Polyimide Covalent Organic Framework Films. *ACS Appl. Mater. Interfaces* **2020,** *12* (46), 51837-51845.
18. Lin, S.; Diercks, C. S.; Zhang, Y. B.; Kornienko, N.; Nichols, E. M.; Zhao, Y.; Paris, A. R.; Kim, D.; Yang, P.; Yaghi, O. M.; Chang, C. J., Covalent organic frameworks comprising cobalt porphyrins for catalytic CO_2 reduction in water. *Science* **2015,** *349* (6253), 1208-1213.
19. Biswal, B. P.; Vignolo-Gonzalez, H. A.; Banerjee, T.; Grunenberg, L.; Savasci, G.; Gottschling, K.; Nuss, J.; Ochsenfeld, C.; Lotsch, B. V., Sustained Solar H_2 Evolution from a Thiazolo[5,4-d]thiazole-Bridged Covalent Organic Framework and Nickel-Thiolate Cluster in Water. *J. Am. Chem. Soc.* **2019,** *141* (28), 11082-11092.
20. Xu, S.; Sun, H.; Addicoat, M.; Biswal, B. P.; He, F.; Park, S.; Paasch, S.; Zhang, T.; Sheng, W.; Brunner, E.; Hou, Y.; Richter, M.; Feng, X., Thiophene-Bridged Donor-Acceptor sp^2-Carbon-Linked 2D Conjugated Polymers as Photocathodes for Water Reduction. *Adv. Mater.* **2021,** *33* (1), 2006274.
21. Han, B.; Ding, X.; Yu, B.; Wu, H.; Zhou, W.; Liu, W.; Wei, C.; Chen, B.; Qi, D.; Wang, H.; Wang, K.; Chen, Y.; Chen, B.; Jiang, J., Two-Dimensional Covalent Organic Frameworks with Cobalt(II)-Phthalocyanine Sites for Efficient Electrocatalytic Carbon Dioxide Reduction. *J. Am. Chem. Soc.* **2021,** *143* (18), 7104-7113.
22. Meng, Z.; Stolz, R. M.; Mirica, K. A., Two-Dimensional Chemiresistive Covalent Organic Framework with High Intrinsic Conductivity. *J. Am. Chem. Soc.* **2019,** *141* (30), 11929-11937.
23. Yue, Y.; Cai, P.; Xu, X.; Li, H.; Chen, H.; Zhou, H. C.; Huang, N., Conductive Metallophthalocyanine Framework Films with High Carrier Mobility as Efficient Chemiresistors. *Angew. Chem., Int. Ed.* **2021,** *60* (19), 10806-10813.

24. Vitaku, E.; Gannett, C. N.; Carpenter, K. L.; Shen, L.; Abruna, H. D.; Dichtel, W. R., Phenazine-Based Covalent Organic Framework Cathode Materials with High Energy and Power Densities. *J. Am. Chem. Soc.* **2020,** *142* (1), 16-20.
25. Singh, V.; Byon, H. R., Advances in electrochemical energy storage with covalent organic frameworks. *Mater. Adv.* **2021,** *2* (10), 3188-3212.
26. Wang, M.; Ballabio, M.; Wang, M.; Lin, H. H.; Biswal, B. P.; Han, X.; Paasch, S.; Brunner, E.; Liu, P.; Chen, M.; Bonn, M.; Heine, T.; Zhou, S.; Canovas, E.; Dong, R.; Feng, X., Unveiling Electronic Properties in Metal-Phthalocyanine-Based Pyrazine-Linked Conjugated Two-Dimensional Covalent Organic Frameworks. *J. Am. Chem. Soc.* **2019,** *141* (42), 16810-16816.
27. Huang, N.; Lee, K. H.; Yue, Y.; Xu, X.; Irle, S.; Jiang, Q.; Jiang, D., A Stable and Conductive Metallophthalocyanine Framework for Electrocatalytic Carbon Dioxide Reduction in Water. *Angew. Chem., Int. Ed.* **2020,** *59* (38), 16587-16593.
28. Jin, E.; Asada, M.; Xu, Q.; Dalapati, S.; Addicoat, M. A.; Brady, M. A.; Xu, H.; Nakamura, T.; Heine, T.; Chen, Q.; Jiang, D., Two-dimensional sp^2 carbon-conjugated covalent organic frameworks. *Science* **2017,** *357* (6352), 673-676.
29. Zhang, B.; Wei, M.; Mao, H.; Pei, X.; Alshmimri, S. A.; Reimer, J. A.; Yaghi, O. M., Crystalline Dioxin-Linked Covalent Organic Frameworks from Irreversible Reactions. *J. Am. Chem. Soc.* **2018,** *140* (40), 12715-12719.
30. Guan, X.; Li, H.; Ma, Y.; Xue, M.; Fang, Q.; Yan, Y.; Valtchev, V.; Qiu, S., Chemically stable polyarylether-based covalent organic frameworks. *Nat. Chem.* **2019,** *11* (6), 587-594.
31. Lu, M.; Zhang, M.; Liu, C. G.; Liu, J.; Shang, L. J.; Wang, M.; Chang, J. N.; Li, S. L.; Lan, Y. Q., Stable Dioxin-Linked Metallophthalocyanine Covalent Organic Frameworks (COFs) as Photo-Coupled Electrocatalysts for CO_2 Reduction. *Angew. Chem., Int. Ed.* **2021,** *60* (9), 4864-4871.
32. Lei, Z.; Lucas, F. W. S.; Canales Moya, E.; Huang, S.; Rong, Y.; Wesche, A.; Li, P.; Bodkin, L.; Jin, Y.; Holewinski, A.; Zhang, W., Highly stable dioxin-linked metallophthalocyanine covalent organic frameworks. *Chin. Chem. Lett.* **2021**, DOI: 10.1016/j.cclet.2021.1004.1047.
33. Medina, D. D.; Werner, V.; Auras, F.; Tautz, R.; Dogru, M.; Schuster, J.; Linke, S.; Doblinger, M.; Feldmann, J.; Knochel, P.; Bein, T., Oriented thin films of a benzodithiophene covalent organic framework. *ACS Nano* **2014,** *8* (4), 4042-4052.
34. Medina, D. D.; Petrus, M. L.; Jumabekov, A. N.; Margraf, J. T.; Weinberger, S.; Rotter, J. M.; Clark, T.; Bein, T., Directional Charge-Carrier Transport in Oriented Benzodithiophene Covalent Organic Framework Thin Films. *ACS Nano* **2017,** *11* (3), 2706-2713.
35. Ghosh, R.; Paesani, F., Unraveling the effect of defects, domain size, and chemical doping on photophysics and charge transport in covalent organic frameworks. *Chem. Sci.* **2021,** *12* (24), 8373-8384.
36. Castano, I.; Evans, A. M.; Reis, R. d.; Dravid, V. P.; Gianneschi, N. C.; Dichtel, W. R., Mapping Grains, Boundaries, and Defects in 2D Covalent Organic Framework Thin Films. *Chem. Mater.* **2021,** *33* (4), 1341-1352.
37. Wang, H.; He, B.; Liu, F.; Stevens, C.; Brady, M. A.; Cai, S.; Wang, C.; Russell, T. P.; Tan, T. W.; Liu, Y., Orientation transitions during the growth of imine covalent organic framework thin films. *J. Mater. Chem. C* **2017,** *5* (21), 5090-5095.
38. Liu, K.; Qi, H.; Dong, R.; Shivhare, R.; Addicoat, M.; Zhang, T.; Sahabudeen, H.; Heine, T.; Mannsfeld, S.; Kaiser, U.; Zheng, Z.; Feng, X., On-water surface synthesis of crystalline, few-layer two-dimensional polymers assisted by surfactant monolayers. *Nat. Chem.* **2019,** *11* (11), 994-1000.
39. Dey, K.; Pal, M.; Rout, K. C.; Kunjattu, H. S.; Das, A.; Mukherjee, R.; Kharul, U. K.; Banerjee, R., Selective Molecular Separation by Interfacially Crystallized Covalent Organic Framework Thin Films. *J. Am. Chem. Soc.* **2017,** *139* (37), 13083-13091.
40. Matsumoto, M.; Valentino, L.; Stiehl, G. M.; Balch, H. B.; Corcos, A. R.; Wang, F.; Ralph, D. C.; Mariñas, B. J.; Dichtel, W. R., Lewis-Acid-Catalyzed Interfacial Polymerization of Covalent Organic Framework Films. *Chem* **2018,** *4* (2), 308-317.
41. Huang, P.; Lethien, C.; Pinaud, S.; Brousse, K.; Laloo, R.; Turq, V.; Respaud, M.; Demortiere, A.; Daffos, B.; Taberna, P. L.; Chaudret, B.; Gogotsi, Y.; Simon, P., On-chip and freestanding elastic carbon films for micro-supercapacitors. *Science* **2016,** *351* (6274), 691-695.
42. Yang, C.; Schellhammer, K. S.; Ortmann, F.; Sun, S.; Dong, R.; Karakus, M.; Mics, Z.; Loffler, M.; Zhang, F.; Zhuang, X.; Canovas, E.; Cuniberti, G.; Bonn, M.; Feng, X., Coordination Polymer Framework Based On-Chip Micro-Supercapacitors with AC Line-Filtering Performance. *Angew. Chem., Int. Ed.* **2017,** *56* (14), 3920-3924.
43. Gimenez-Marques, M.; Bellido, E.; Berthelot, T.; Simon-Yarza, T.; Hidalgo, T.; Simon-Vazquez, R.; Gonzalez-Fernandez, A.; Avila, J.; Asensio, M. C.; Gref, R.; Couvreur, P.; Serre, C.; Horcajada, P., GraftFast Surface Engineering to Improve MOF Nanoparticles Furtiveness. *Small* **2018,** *14* (40), 1801900.
44. Frati, F.; Hunault, M.; de Groot, F. M. F., Oxygen K-edge X-ray Absorption Spectra. *Chem. Rev.* **2020,** *120* (9), 4056-4110.
45. Wu, S.; Wang, W.; Li, M.; Cao, L.; Lyu, F.; Yang, M.; Wang, Z.; Shi, Y.; Nan, B.; Yu, S.; Sun, Z.; Liu, Y.; Lu, Z., Highly durable organic electrode for sodium-ion batteries via a stabilized α-C radical intermedia. *Nat. Commun.* **2016,** *7*, 13318.
46. Yang, C.; Dong, R.; Wang, M.; Petkov, P. S.; Zhang, Z.; Wang, M.; Han, P.; Ballabio, M.; Brauninger, S. A.; Liao, Z.; Zhang, J.; Schwotzer, F.; Zschech, E.; Klauss, H. H.; Canovas, E.; Kaskel, S.; Bonn, M.; Zhou, S.; Heine, T.; Feng, X., A semiconducting layered metal-organic framework magnet. *Nat. Commun.* **2019,** *10* (1), 3260.
47. Jin, S.; Ding, X.; Feng, X.; Supur, M.; Furukawa, K.; Takahashi, S.; Addicoat, M.; El-Khouly, M. E.; Nakamura, T.; Irle, S.; Fukuzumi, S.; Nagai, A.; Jiang, D., Charge dynamics in a donor-acceptor covalent organic framework with periodically ordered bicontinuous heterojunctions. *Angew. Chem., Int. Ed.* **2013,** *52* (7), 2017-2021.
48. Elbourne, A.; McDonald, S.; Voichovsky, K.; Endres, F.; Warr, G. G.; Atkin, R., Nanostructure of the Ionic Liquid-Graphite Stern Layer. *ACS Nano* **2015,** *9* (7), 7608-7620.
49. Wang, J.; Polleux, J.; Lim, J.; Dunn, B., Pseudocapacitive Contributions to Electrochemical Energy Storage in TiO_2 (Anatase) Nanoparticles. *J. Phys. Chem. C* **2007,** *111* (40), 14925-14931.
50. Jiang, Y.; Liu, J., Definitions of Pseudocapacitive Materials: A Brief Review. *Energy Environ. Mater.* **2019,** *2* (1), 30-37.
51. Ardizzone, S.; Fregonara, G.; Trasatti, S., "Inner" and "outer" active surface of RuO_2 electrodes. *Electrochim. Acta* **1990,** *35* (1), 263-267.
52. Zhang, L.; Zhang, F.; Yang, X.; Long, G.; Wu, Y.; Zhang, T.; Leng, K.; Huang, Y.; Ma, Y.; Yu, A.; Chen, Y., Porous 3D graphene-based bulk materials with exceptional high surface area and excellent conductivity for supercapacitors. *Sci. Rep.* **2013,** *3*, 1408.
53. Izadi-Najafabadi, A.; Yasuda, S.; Kobashi, K.; Yamada, T.; Futaba, D. N.; Hatori, H.; Yumura, M.; Iijima, S.; Hata, K., Extracting the full potential of single-walled carbon nanotubes as durable supercapacitor electrodes operable at 4 V with high power and energy density. *Adv. Mater.* **2010,** *22* (35), 235-241.
54. Zhu, Y.; Murali, S.; Stoller, M. D.; Ganesh, K. J.; Cai, W.; Ferreira, P. J.; Pirkle, A.; Wallace, R. M.; Cychosz, K. A.; Thommes, M.; Su, D.; Stach, E. A.; Ruoff, R. S., Carbon-based supercapacitors produced by activation of graphene. *Science* **2011,** *332* (6037), 1537-1541.

Table of Contents Artwork